

# Light-shinning-through-thin-wall radio frequency cavities for probing dark photon

Dmitry Salnikov,<sup>\*</sup> Petr Satunin,<sup>†</sup> and Leysan Valeeva<sup>‡</sup>  
*Moscow State University, 119991 Moscow, Russia and  
 Institute for Nuclear Research, 117312 Moscow, Russia*

D. V. Kirpichnikov<sup>§</sup>  
*Institute for Nuclear Research, 117312 Moscow, Russia*  
 (Dated: February 16, 2024)

We address the radio frequency (RF) cavity experiment for probing dark photons which is a modification of the light-shining-through-thin-wall (LStinW) setup with a relatively thin conducting barrier between cylindrical emitter and hollow receiver. The regarding experimental facility allows to probe dark photons effectively even in the off-shell regime, i. e. when dark photons mass exceeds the driven frequency of the emitter cavity, that is pumped by electromagnetic mode. We compare the sensitivity of two concrete setup configurations: two cylindrical cavities placed to each other by an end-caps, and nested geometry of the cavities in which the cylindrical receiver is encapsulated into the emitter. We show that for a certain range of dark photon mass the nested configuration can provide an enhanced sensitivity if one compares that with a separated emitter setup.

## I. INTRODUCTION

A dark (hidden) photon is a massive hypothetical particle that interacts with the Standard Model (SM) through kinetic mixing with a visible photon [1]. For relatively small values of the kinetic mixing parameter, dark photon (DP) can avoid cosmological constraints and thus it can be a viable candidate for the dark matter [2, 3]. It is worth noticing, a hidden photon is addressed also in the scenarios as a mediator between dark matter and visible sector [4–6]. Typically a DP is described in the framework of  $U(1)$  gauge extension of SM, that is natural requirement for a string theory [7].

A variety of precise searches for hidden photon have been carried out recently in numerous laboratory and accelerator based experiments. For instance, a searches for hidden photons with relatively heavy masses (in the  $\lesssim \mathcal{O}(1)$  GeV range) have utilized  $e^+e^-$  [8] and  $pp$  colliders [9], the NA64 fixed target [10, 11], the JUNO underground detectors [12], and FASER beam-dump [13] experiments.

In addition, we also address the low mass limits (sub  $\sim \mathcal{O}(1)$  eV range) derived from tests of Coulomb's law [14, 15] and atomic spectroscopy [16]. The limits on dark photons that can be hypothetical DM candidates are performed in haloscope searches [17–25], gravitational wave detector [26], cryogenic millimeter-wave cavity [27], dish antenna [28], radio telescopes [29], gaseous

detectors [30], photonic chip [31], astrophysical environments [32], and Earth-based magnetometers [33, 34] (for recent review see also Ref. [35] and references therein).

For completeness, it is worth noticing that a dark photons for the sufficiently small masses below  $\lesssim 1$  eV have been probed with the SM photon regeneration facilities such as DarkSRF [36], CROWS [37], ADMX [38], and microwave cavity experiment [39]. The latter facilities are referred to light-shining-through-wall (LSW) experiments. To be more specific, the regarding detection schemes to search for dark photons are associated with electromagnetically isolated conducting cavities tuned to the same frequency [40, 41]. In particular, a dark photons produced from high-density SM photons in the emitter cavity propagate in space until reaching the other receiver hollow cavity where they convert back into SM photons.

The authors of Ref. [42] argued that, while previous literature [37, 39, 41, 43–45] focused on the production and detection of transverse modes of hidden photon, the longitudinal mode allows a significant improvement in LSW experimental sensitivity. In the present paper we employ the formalism of Ref. [42] in order to calculate the sensitivity of cylindrical receiver that is nested (or encapsulated) inside the emitter cavity [43] (see e. g. Fig. 1 for detail) for sufficiently thin wall between receiver and emitter [46]. The similar experimental setup is addressed in Ref. [46] as light-shining-through-thin-wall (LStinW) but for distant cylindrical cavities (see e. g. Fig. 2 for detail). The typical barrier between endcaps of the receiver and emitter cavity [46] is sufficiently small  $d \simeq \mathcal{O}(10) \mu\text{m} \ll 1/\omega$ , where  $\omega \sim \mathcal{O}(1)$  GHz  $\sim \mathcal{O}(1) \mu\text{eV}$  is a typical driven radio frequency (RF) of the emitter pump mode (it matches with a signal EM mode frequency that is resonantly induced in the hollow receiver).

<sup>\*</sup> e-mail: [salnikov.dv16@physics.msu.ru](mailto:salnikov.dv16@physics.msu.ru); corresponding author

<sup>†</sup> e-mail: [petr.satunin@gmail.com](mailto:petr.satunin@gmail.com)

<sup>‡</sup> e-mail: [valeeva.ln19@physics.msu.ru](mailto:valeeva.ln19@physics.msu.ru)

<sup>§</sup> e-mail: [dmbriick@gmail.com](mailto:dmbriick@gmail.com); corresponding author

The LStinW setup allows to enhance the sensitivity in the off-shell DP region, i. e. when hidden photon mass,  $m_{A'}$ , is relatively large  $m_{A'} \gg \omega$ . In addition, employing the sufficiently low driven frequency of the emitter, one can achieve a large density of the source photons and high quality of the superconducting RF (SRF) cavity [46].

In the present paper, we estimate the impact on the DP sensitivity that is associated with the wall thickness  $d$  between cavities for the nested design of LStinW setup shown in Fig. 1. We also show that there is an advantage of nested receiver as opposed to its distant location Fig. 2 for the specific resonator design.

This paper is organized as follows. In Sec. II we discuss general properties of DP scenario and derive regarding equations of motion. In Sec. III we derive a signal power that implies probing the DP in the SRF receiver. In Sec. IV we calculate overlapping factor for distant location of receiver and emitter, while in Sec. V we derive the form-factor expression for the cylindrical receiver that is nested in the emitter. In Sec. VI we estimate the sensitivity of the aforementioned LStinW designs. In Appendix A and B we specify some useful formulas for the form-factor derivation in the analytical form.

## II. FRAMEWORK OF THE SCENARIO

Let us consider the Lagrangian, describing a coupling of the ordinary Standard Model (SM) photon,  $\hat{A}_\mu$ , with a massive vector hidden state,  $\hat{A}'_\mu$ , through the kinetic mixing

$$\mathcal{L} \supset -\frac{1}{4}\hat{F}_{\mu\nu}^2 - \frac{1}{4}\left(\hat{F}'_{\mu\nu}\right)^2 + \frac{1}{2}m_{A'}^2\left(\hat{A}'_\mu\right)^2 + \frac{\epsilon}{2}\hat{F}'_{\mu\nu}\hat{F}^{\mu\nu} - J_\mu\hat{A}^\mu, \quad (1)$$

where we exploit the hat over the boson fields in order to label the states of the benchmark interaction Eq. (1) in so called *field basis* [42] or *kinetically mixed basis* [34],  $\epsilon$  is a dimensionless coupling of the kinetic mixing, that is assumed to be small,  $\epsilon \ll 1$ ,  $\hat{F}_{\mu\nu}^{(\prime)}$  is the stress tensor of the (dark) photon,  $J^\mu$  is the typical  $U(1)$  electromagnetic current density. Now let us get rid of the non-diagonal kinetic mixing term  $\propto \epsilon$  in Eq. (1) by the following replacement of the field basis states  $\hat{A}_\mu^{(\prime)}$  to the *mass basis states*  $A_\mu^{(\prime)}$ ,

$$\hat{A}_\mu = A_\mu + \frac{\epsilon}{\sqrt{1-\epsilon^2}}A'_\mu, \quad \hat{A}'_\mu = \frac{1}{\sqrt{1-\epsilon^2}}A'_\mu, \quad (2)$$

as a result, one gets the following redefined Lagrangian

$$\mathcal{L} \supset -\frac{1}{4}F_{\mu\nu}^2 - \frac{1}{4}(F'_{\mu\nu})^2 + \frac{1}{2}\frac{m_{A'}^2}{(1-\epsilon^2)}(A'_\mu)^2 - J_\mu\left(A^\mu + \frac{\epsilon}{\sqrt{1-\epsilon^2}}A'^\mu\right), \quad (3)$$

that leads to the decoupled equations of motions for both  $A_\mu$  and  $A'_\mu$

$$\partial_\mu^2 A_\nu = J_\nu, \quad (4)$$

$$\partial_\mu^2 A'_\nu + \frac{m_{A'}^2}{1-\epsilon^2}A'_\nu = \frac{\epsilon}{(1-\epsilon^2)}J_\nu, \quad (5)$$

where we impose the Lorentz gauge  $\partial_\mu A^\mu = 0$  and on-shell Proca condition  $\partial_\mu A'^\mu = 0$ , implying that it leads to conservation of the electromagnetic current  $\partial_\mu J^\mu = 0$  (see e. g. Ref. [34] for detail). The electric and magnetic fields are defined in a usual manner for both SM,  $A_\mu$ , and hidden photon,  $A'_\mu$ ,

$$\mathbf{E}^{(\prime)} = -\nabla\phi^{(\prime)} - \partial_t\mathbf{A}^{(\prime)}, \quad \mathbf{B}^{(\prime)} = \nabla \times \mathbf{A}^{(\prime)}, \quad (6)$$

where we imply the typical four-vector notation via potential,  $A^{(\prime)0} \equiv \phi^{(\prime)}$  and vector terms  $A^{(\prime)i} \equiv \mathbf{A}^{(\prime)}$ . However, it was pointed out in Ref. [42] that in order to calculate the physical state propagation one should express the fields in the mass basis through the linear combination of the *visible*,  $A_{\text{vis}}^\mu$ , and *invisible*,  $A_{\text{inv}}^\mu$ , modes in the following form [46]

$$A^\mu = \sqrt{1-\epsilon^2}A_{\text{vis}}^\mu - \epsilon A_{\text{inv}}^\mu, \quad (7)$$

$$A'^\mu = \epsilon A_{\text{vis}}^\mu + \sqrt{1-\epsilon^2}A_{\text{inv}}^\mu. \quad (8)$$

As a result, for the regarding basis, the equations of motions (4) and (5) can be rewritten as follows

$$(\partial_t^2 - \nabla^2)A_{\text{vis}}^\mu = J_{\text{SM}}^\mu - \frac{\epsilon m_{A'}^2}{(1-\epsilon^2)}A'^\mu \quad (9)$$

$$\left(\partial_t^2 - \nabla^2 + \frac{m_{A'}^2}{(1-\epsilon^2)}\right)A_{\text{inv}}^\mu = -\frac{\epsilon m_{A'}^2}{(1-\epsilon^2)}A^\mu, \quad (10)$$

where we use convention for the effective SM density current  $J_{\text{SM}}^\mu \equiv \sqrt{1-\epsilon^2}J^\mu$ . In Eqs. (9) and (10) we keep the dependence on  $A'^\mu$  and  $A^\mu$  in the right hand side respectively in order to emphasize, that at the leading order approach,  $\epsilon \ll 1$ , the visible component  $A_{\text{vis}}^\mu$  is sourced by the electromagnetic SM current  $J_{\text{SM}}^\mu$ . Moreover, the invisible mode  $A_{\text{inv}}^\mu$  is sourced only by the typical effective current  $\propto -\epsilon m_{A'}^2 A^\mu$ , that is subdominant to the  $J_{\text{SM}}^\mu$ .

## III. CAVITY RESPONSE

Let us consider benchmark experimental setups consisting of the high-quality superconducting RF cylindrical receiver cavity which is

- separated from the emitter by the thin barrier of  $d \ll R$ , where  $R = R_{\text{em}} = R_{\text{rec}}$  is a typical radius of the cavities (see Fig. 2);

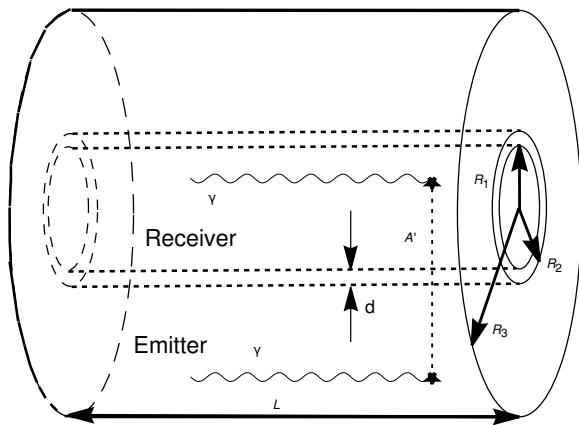


FIG. 1. Typical sketch of the cavity setup with the encapsulated receiver.

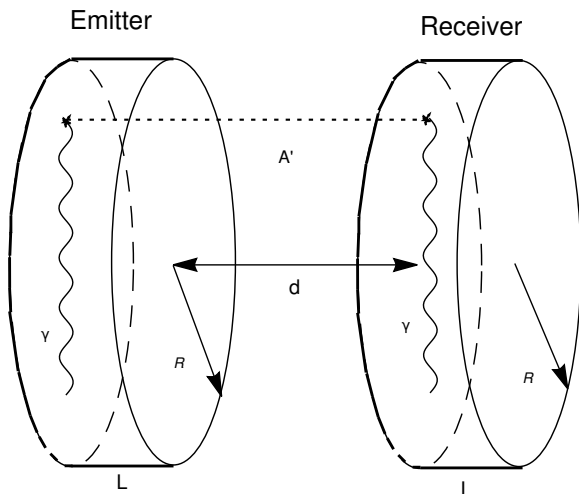


FIG. 2. Typical scheme of the setup for distant cavities. We note that a realistic configuration implies thin conducting barrier between cavities such that  $d \ll R, L$ .

- nested into emitter such that they have common perfectly conducting thin side wall of thickness  $d \ll R$  (see Fig. 1).

Let  $\mathbf{x}$  and  $\mathbf{y}$  be the coordinates associated with the emitter and receiver frame respectively. In addition, let  $\mathbf{l}$  be the vector linking the origins of the frames of both emitter and receiver for the coaxial design of the experimental setup. In this case one has a simple link between

them  $\mathbf{x} = \mathbf{l} + \mathbf{y}$ .

The first cavity is pumped by a single electromagnetic mode (EM)

$$\mathbf{E}(\mathbf{x}, t) = \mathbf{E}_{\text{em}}(\mathbf{x})e^{-i\omega t}, \quad (11)$$

$$\mathbf{B}(\mathbf{x}, t) = \mathbf{B}_{\text{em}}(\mathbf{x})e^{-i\omega t}, \quad (12)$$

oscillating at frequency  $\omega$  and serves as an emitter of dark photon. In (11) and (12) we employ convention of [47] for the time dependence  $\propto e^{-i\omega t}$  in order to match the notation of cavity eigenmodes [47]. The second cavity is a quiet hollow receiver of dark photon, thus it is expected that the detecting EM mode is resonantly excited due to regeneration of hidden vector state radiated from the emitter cavity.

Now let us define the invisible electric field  $\mathbf{E}_{\text{inv}} \equiv \mathbf{E}' - \epsilon\mathbf{E}$ , this means that Eq. (10) implies the following massive wave equation

$$(\partial_t^2 - \nabla^2 + m_{A'}^2) \mathbf{E}_{\text{inv}} = -\epsilon m_{A'}^2 \mathbf{E}. \quad (13)$$

The Eq. (13) means that the invisible electric field inside the receiver cavity sourced by the massless field of the emitter  $\mathbf{E} = \mathbf{E}_{\text{em}}e^{-i\omega t}$ . At the order of  $\mathcal{O}(\epsilon)$  one has  $\mathbf{E}_{\text{inv}} \simeq \mathbf{E}'$  and thus the dark photon electric mode in the receiver can be expressed via Green's function in the following form [42]

$$\mathbf{E}'(\mathbf{x}, t) = -\frac{\epsilon m_{A'}^2}{4\pi} \int_{V_{\text{em}}} d^3\mathbf{x}' \frac{e^{-i\omega t + ik_{A'}|\mathbf{x} - \mathbf{x}'|}}{|\mathbf{x} - \mathbf{x}'|} \mathbf{E}_{\text{em}}(\mathbf{x}'), \quad (14)$$

where integration  $d^3\mathbf{r}'$  is performed over the emitter cavity volume  $V_{\text{em}}$  for the emitter frame,  $k_{A'}$  is a wavenumber that reads as  $k_{A'} \equiv \sqrt{\omega^2 - m_{A'}^2}$  for relatively small masses  $m_{A'} \lesssim \omega$  and  $k_{A'} = i\kappa_{A'}$  with  $\kappa_{A'} \equiv \sqrt{m_{A'}^2 - \omega^2}$  for heavy hidden vector state  $m_{A'} \gtrsim \omega$ .

Now let us estimate the resonant response of the receiver cavity. We define first the visible electric field as  $\mathbf{E}_{\text{vis}} \equiv \mathbf{E} + \epsilon\mathbf{E}'$  that obeys the following boundary condition on the conducting surface

$$[\mathbf{n} \times \mathbf{E}_{\text{vis}}] \Big|_{\partial V_{\text{rec}}} = 0, \quad (15)$$

where the unit vector  $\mathbf{n}$  is defined along the normal to the interior bound  $\partial V_{\text{rec}}$  of the receiver cavity [42]. One can show [42] that at leading order  $\mathcal{O}(\epsilon)$  the receiver response  $\mathbf{E}_{\text{vis}}$  sourced by the time derivative of the typical effective current

$$\nabla \times (\nabla \times \mathbf{E}_{\text{vis}}) + \partial_t^2 \mathbf{E}_{\text{vis}} = -\partial_t \mathbf{J}_{\text{eff}}(\mathbf{y}, t), \quad (16)$$

where the left hand side equations imply the derivatives with respect to the receiver frame  $\mathbf{y}$ ,  $\partial_t \mathbf{J}_{\text{eff}}(\mathbf{x}, t) = -i\omega \mathbf{J}_{\text{eff}}(\mathbf{x})e^{-i\omega t}$ , here the stationary part of the regaining current reads as follows

$$\mathbf{J}_{\text{eff}}(\mathbf{x}) = \frac{\epsilon}{i\omega} [\nabla \cdot (\nabla \cdot \mathbf{E}'(\mathbf{x})) - m_{A'}^2 \mathbf{E}'(\mathbf{x})], \quad (17)$$

where  $\mathbf{E}'(\mathbf{x})$  is a spatial profile term of Eq. (14). The solution to Eq. (16) for the receiver can be expressed in the following form

$$\mathbf{E}_{\text{vis}}(\mathbf{y}, t) \simeq -\frac{Q}{\omega_n} \mathbf{E}_{\text{rec}}^{(n)}(\mathbf{y}) e^{-i\omega t} \times \frac{\int_{V_{\text{rec}}} d^3\mathbf{y}' \left( \mathbf{E}_{\text{rec}}^{(n)*}(\mathbf{y}') \cdot \mathbf{J}_{\text{eff}}(\mathbf{y}') \right)}{\int_{V_{\text{rec}}} d^3\mathbf{y}' |\mathbf{E}_{\text{rec}}^{(n)}(\mathbf{y}')|^2}, \quad (18)$$

where  $\mathbf{E}_{\text{rec}}^{(n)}(\mathbf{y})$  is divergence-free vacuum cavity-mode,  $\nabla \cdot \mathbf{E}_{\text{rec}}^{(n)}(\mathbf{y}) = 0$ ,  $Q$  is a quality factor of the receiver cavity,  $\omega_n$  is a cavity eigen-frequency that is closed to the driven frequency  $\omega_n \simeq \omega$  in the resonant response regime, i. e. when the signal build up time  $t$  is sufficiently large  $t \gg Q/\omega$ . The quality factor is chosen to be  $Q \simeq 4 \times 10^{10}$  throughout the paper. We notice again for completeness, that the integration over  $d^3\mathbf{y}'$  in Eq. (18) is performed over the receiver cavity volume  $V_{\text{rec}}$  in the receiver frame  $\mathbf{y}'$ .

One can show [48] that the total energy stored in the receiver cavity due to the resonant response is

$$W_{\text{rec}} \simeq \frac{1}{2} \int_{V_{\text{rec}}} d^3\mathbf{y} \left[ \langle \text{Re}[\mathbf{B}_{\text{vis}}(\mathbf{y}, t)]^2 \rangle_t + \langle \text{Re}[\mathbf{E}_{\text{vis}}(\mathbf{y}, t)]^2 \rangle_t \right] \quad (19)$$

where we employ the time averaging notations  $\langle \dots \rangle_t$  for the energy density of both the magnetic,  $\propto \langle \text{Re}[\mathbf{B}_{\text{vis}}(\mathbf{y}, t)]^2 \rangle_t/2$ , and electric,  $\propto \langle \text{Re}[\mathbf{E}_{\text{vis}}(\mathbf{y}, t)]^2 \rangle_t/2$  fields in the perfect conductor, here  $\text{Re}[\dots]$  is a real part of the EM fields. Remarkably, the regarding energy densities are equal in the resonant regime [48], and the resulted expression for  $W_{\text{rec}}$  can be expressed only through the integral over the electric energy density  $\propto |\mathbf{E}_{\text{vis}}(\mathbf{y})|^2/2$  term, where  $\mathbf{E}_{\text{vis}}(\mathbf{y})$  is a stationary part of Eq. (18).

From the discussion above one can estimate the signal power emission of a cavity

$$P_{\text{sign}} \simeq \frac{\omega}{Q} W_{\text{rec}} = \frac{\omega}{2Q} \int_{V_{\text{rec}}} d^3\mathbf{y} |\mathbf{E}_{\text{vis}}(\mathbf{y})|^2 = \frac{Q}{2\omega} |\mathcal{G}|^2, \quad (20)$$

where  $\mathcal{G}$  is a overlapping factor (here we keep it dimensional for brevity)

$$\mathcal{G} = \frac{\int_{V_{\text{rec}}} d^3\mathbf{y} \left( \mathbf{E}_{\text{rec}}^{(n)*}(\mathbf{y}) \cdot \mathbf{J}_{\text{eff}}(\mathbf{y}) \right)}{\left( \int_{V_{\text{rec}}} d^3\mathbf{y} |\mathbf{E}_{\text{rec}}^{(n)}(\mathbf{y})|^2 \right)^{1/2}}. \quad (21)$$

It is worth noticing Eq. (21) implies that the signal is agnostic to overall constant normalization pre-factor of the receiver mode,  $\mathbf{E}_{\text{rec}}^{(n)}(\mathbf{y})$ , however it depends on the specific mode type and the overlapping integrals in the numerator and denominator of Eq. (21).

We estimate the sensitivity as an maximum output in the receiver that is defined by the Dickie radiometer equation [49],

$$\text{SNR} = \frac{P_{\text{sign}}}{P_{\text{noise}}} \sqrt{t\Delta\nu}, \quad (22)$$

where  $t$  is an integration time of the signal,  $\Delta\nu$  is a signal bandwidth,  $P_{\text{noise}}$  is a power of thermal noise that is estimated to be  $P_{\text{noise}} \simeq T\Delta\nu$  for  $\omega \ll T$ . The typical temperature of the receiver is chosen to be  $T \simeq 4$  K. It is worth noticing that the narrowest possible bandwidth can be as small as  $\Delta\nu \simeq 1/t$ , thus in the numerical estimation we conservatively set integration time to be  $t \simeq 1$  year.

Let us present the general formula to calculate the sensitivity for the mixing parameter  $\epsilon$  for the specific cavity geometry,

$$\epsilon = \left( \frac{2T \cdot \text{SNR}}{Q\omega^3 (E_{\text{em}}^0)^2 V_{\text{em}}^2 V_{\text{rec}}} \right)^{\frac{1}{4}} \left( \frac{\Delta\nu}{t} \right)^{\frac{1}{8}} m_{A'}^{-1} |\tilde{\mathcal{G}}|^{-1/2}. \quad (23)$$

where  $\tilde{\mathcal{G}}$  is a dimensionless geometric factor,

$$\tilde{\mathcal{G}} = \frac{1}{\omega^3} \int_{V_{\text{rec}}} \frac{d^3\mathbf{y}}{V_{\text{rec}}} \int_{V_{\text{em}}} \frac{d^3\mathbf{x}}{V_{\text{em}}} \mathcal{E}_{\text{rec}}^{*i}(\mathbf{y}) \mathcal{E}_{\text{em}}^j(\mathbf{x}) \times \left( m_{A'}^2 \delta_{ij} - \partial_{y_i} \partial_{y_j} \right) \left\{ -\frac{\exp(ik_{A'}|\mathbf{x} - \mathbf{y} - \mathbf{l}|)}{4\pi|\mathbf{x} - \mathbf{y} - \mathbf{l}|} \right\}, \quad (24)$$

where  $\mathcal{E}_{\text{rec}}^i(\mathbf{y})$  and  $\mathcal{E}_{\text{em}}^i(\mathbf{x})$  are cavity modes of the receiver and emitter respectively which are connected with electric fields as follows

$$E_{\text{em}}^i(\mathbf{x}) = E_{\text{em}}^0 \cdot \mathcal{E}_{\text{em}}^i(\mathbf{x}), \quad (25)$$

$$E_{\text{rec}}^i(\mathbf{y}) = \mathcal{E}_{\text{rec}}^i(\mathbf{y}), \quad (26)$$

where  $E_{\text{em}}^0$  is a magnitude of the driven emitter electric field, indices  $i$  and  $j$  label the  $i^{\text{th}}$  and  $j^{\text{th}}$  components of the electric field respectively. In the present paper we set the typical driving EM field to be  $E_{\text{em}}^0 = 30$  MV/m = 0.1 T (see e. g. Ref. [46] for detail). In addition we introduce the pre-factor  $1/\omega^3$  in Eq. (24) in order to obtain dimensionless form-factor  $\tilde{\mathcal{G}}$ . In order to estimate the expected reach of the experimental configuration, we put  $\text{SNR} \simeq 5$  in Eq. (23).

In addition we note that eigenmodes are normalized as follows

$$\int_{V_{\text{rec/em}}} d^3\mathbf{r} |\mathcal{E}_{\text{rec/em}}^i(\mathbf{r})|^2 = V_{\text{rec/em}}. \quad (27)$$

In Eq. (26) we omit the amplitude of the of receiver field for brevity (see e. g. discussion after Eq. (21) for details).

#### IV. COAXIAL DISTANT CAVITIES: TM<sub>010</sub> MODE

In this section we consider the experimental design of two coaxial distant cavities shown in Fig. 2. The vector linking the cavity frames would be then  $\mathbf{l} = (0, 0, l_z)$ . For that notation the distance between closest endcaps of the cavities is  $d = l_z - L$ . We consider the TM<sub>010</sub> mode of the receiver and emitter. This mode implies the following non-zero electric field components along  $z$ -direction

$$\mathcal{E}_{z,\text{em}}^{\text{TM}_{010}}(\rho, \phi, z) = J_0(k_{1\rho}\rho) / J_1(\omega R), \quad (28)$$

$$\mathcal{E}_{z,\text{rec}}^{\text{TM}_{010}}(\rho', \phi', z') = J_0(k_{1\rho}\rho') / J_1(\omega R), \quad (29)$$

where  $(\rho, \phi, z)$  and  $(\rho', \phi', z')$  are the cylindrical coordinates associated with emitter and receiver frame respectively,  $k_{1\rho}$  is ratio  $k_{1\rho} = x_{01}/R$  with  $x_{01}$  being a first zero of Bessel function,  $J_0(x_{01}) = 0$ . We take into account in Eqs. (28) and (29) that tangential component of the electric field is zero on the conducting surface (15).

It is worth noticing that employing  $\mathbf{k}$  momentum representation of the spherical Green's function

$$\frac{e^{ik_{A'}|\mathbf{x}-\mathbf{y}-\mathbf{l}|}}{4\pi|\mathbf{x}-\mathbf{y}-\mathbf{l}|} = - \int \frac{d^3\mathbf{k}}{(2\pi)^3} \frac{e^{-i\mathbf{k}(\mathbf{x}-\mathbf{y}-\mathbf{l})}}{\mathbf{k}^2 - (k_{A'}^2 + i\varepsilon)}, \quad (30)$$

one can rewrite overlapping factor involving the nonzero effective current component  $J_{\text{eff}}^z(\mathbf{x}) \neq 0$  in Eq. (21) in the following form

$$\begin{aligned} \tilde{\mathcal{G}} &= \frac{1}{\omega^3 V_{\text{rec}} V_{\text{em}}} \int_{V_{\text{rec}}} d^3\mathbf{y} \int_{V_{\text{em}}} d^3\mathbf{x} \frac{d^3\mathbf{k}}{(2\pi)^3} \times \\ &\times \mathcal{E}_{z,\text{rec}}^{\text{TM}_{010}}(\mathbf{y}) \mathcal{E}_{z,\text{em}}^{\text{TM}_{010}}(\mathbf{x}) \frac{(k_z^2 + m_{A'}^2) e^{-i\mathbf{k}(\mathbf{x}-\mathbf{y}-\mathbf{l})}}{[\mathbf{k}^2 - k_{A'}^2 - i\varepsilon]}, \end{aligned} \quad (31)$$

where we imply that the integration over  $d^3\mathbf{k}$  is performed for cylindrical frame, in addition we note that a small complex contribution from  $+i\varepsilon$  in the denominator of Eq. (31) is crucial for spherical wave Fourier transformation in Eq. (14). Remarkably, the 9D integral for the overlapping factor (31) can be reduced to the simplified form

$$\tilde{\mathcal{G}} = \frac{L^2 R^2}{\omega V_{\text{rec}} V_{\text{em}}} \times \mathcal{I}, \quad (32)$$

where  $\mathcal{I}$  can be expressed through the 2D integral

$$\begin{aligned} \mathcal{I} &= \int_0^\infty dk_\rho k_\rho \frac{J_0^2(k_\rho R)}{(k_\rho^2 - \omega^2)^2} \\ &\times \int_{-\infty}^\infty dk_z \frac{4 \sin^2(k_z L/2) (k_z^2 + m_{A'}^2) e^{ik_z l_z}}{L^2 k_z^2 (k_z^2 - [k_{A'}^2 - k_\rho^2 + i\varepsilon])}. \end{aligned} \quad (33)$$

In order to obtain Eq. (33) from Eq. (31) one can exploit the helpful integrals that are collected in Appendix A. Furthermore, the calculation of the second term in Eqs. (33) is straightforward for  $d \equiv l_z - L \gtrsim 0$ , since the  $k_z$ -complex integration contour can be closed upward in order to pick up pole in this case. In particular, for  $k_{A'}^2 \equiv \omega^2 - m_{A'}^2 \gtrsim 0$ , the integration over  $k_z$  splits into a sum of two terms,  $\mathcal{I} = \mathcal{I}[k_\rho \gtrsim k_{A'}] + \mathcal{I}[k_\rho \lesssim k_{A'}]$ , where

$$\begin{aligned} \mathcal{I}[k_\rho \gtrsim k_{A'}] &= 2\pi k_{A'} \int_0^\infty dx \frac{J_0^2(k_{A'} R \sqrt{1+x^2})}{(\omega^2 - k_{A'}^2 (1+x^2))} \\ &\times \frac{4 \sinh^2(x k_{A'} L/2)}{2(k_{A'} x L)^2} \exp(-x k_{A'} l_z) \end{aligned} \quad (34)$$

is a term that is associated with the typical region  $k_\rho \gtrsim k_{A'}$  implying the variable redefinition  $k_\rho = k_{A'}(1+x^2)^{1/2}$  in the integrand, and

$$\begin{aligned} \mathcal{I}[k_\rho \lesssim k_{A'}] &= 2\pi i k_{A'} \int_0^1 dx \frac{J_0^2(k_{A'} R \sqrt{1-x^2})}{(\omega^2 - k_{A'}^2 (1-x^2))} \\ &\times \frac{4 \sin^2(x k_{A'} L/2)}{2(k_{A'} x L)^2} \exp(i x k_{A'} l_z) \end{aligned} \quad (35)$$

is a term that corresponds to the  $k_z$  integration with the typical parametric area  $k_\rho \lesssim k_{A'}$  for the variable replacement  $k_\rho = k_{A'}(1-x^2)^{1/2}$ . Moreover, for TM<sub>010</sub> mode both Eqs. (34) and (35) imply that  $\omega = k_{1\rho} \equiv x_{01}/R$ . For  $\varkappa_{A'}^2 \equiv m_{A'}^2 - \omega^2 \gtrsim 0$  the overlapping factor simply reads as

$$\begin{aligned} \mathcal{I} &= 2\pi \varkappa_{A'} \int_1^\infty dx \frac{J_0^2(\varkappa_{A'} R \sqrt{x^2-1})}{(\omega^2 - \varkappa_{A'}^2 (x^2-1))} \\ &\times \frac{4 \sinh^2(x \varkappa_{A'} L/2)}{2(\varkappa_{A'} x L)^2} \exp(-x \varkappa_{A'} l_z), \end{aligned} \quad (36)$$

where we use the integration variable replacement  $k_\rho = \varkappa_{A'}(x^2-1)^{1/2}$ . The asymptotic of  $\tilde{\mathcal{G}}$  in the sufficiently large masses region  $m_{A'} \gg 1/d \gtrsim \omega$  for the distant cavity design is estimated to be (see e. g. Appendix B for detail)

$$\tilde{\mathcal{G}} \propto \frac{e^{-m_{A'} d}}{(m_{A'})^{7/2}}, \quad (37)$$

as a result of Eq. (37) one has

$$\epsilon \propto (m_{A'})^{3/4} \times e^{-\frac{m_{A'} d}{2}} \quad (38)$$

for the distant setup.

#### V. COAXIAL ENCAPSULATED CAVITY: TM<sub>010</sub> MODE

In this section we consider the following design of the light-shining-through-wall experimental setup shown in

Fig. 1. The emitter is space between internal and external coaxial cylindrical hollow superconducting cavities of radius  $R_2$  and  $R_3$  respectively. The receiver is an internal hollow cylindrical cavity of radius  $R_1$  that is encapsulated into emitter. Both external and internal cavities have an equal length  $L$ , moreover the origins of their frames coincide, such that, one should set  $\mathbf{I} \equiv \mathbf{0}$  in Eq. (21). We suppose that the thickness of the superconducting wall between cavities [46] is sufficiently small  $d \equiv R_2 - R_1 \ll R_3 \simeq \mathcal{O}(10)\text{cm}$ . We note that Eqs. (15) and (29) imply that the electric field mode of the cylindrical receiver is given by

$$\mathcal{E}_{z,\text{rec}}^{\text{TM}_{010}}(\rho', \phi', z') = J_0(\omega\rho')/J_1(\omega R_1), \quad (39)$$

where  $\omega = x_{01}/R_1$  is a eigen-frequency of  $\text{TM}_{010}$  mode. The emitter electric field can be expressed through the specific cylindrical function  $Z_0(x)$  in the following form,

$$\begin{aligned} \mathcal{E}_{z,\text{em}}^{\text{TM}_{010}}(\rho, \phi, z) & \quad (40) \\ &= \beta \left( J_0(\omega\rho) - \frac{J_0(\omega R_2)}{Y_0(\omega R_2)} \cdot Y_0(\omega\rho) \right) \equiv \beta Z_0(\omega\rho), \end{aligned}$$

where  $Y_0(x)$  is the Neumann function of zeroth order. The pre-factor  $\beta$  in Eq. (40) can be obtained from the normalization integral Eq. (27),

$$\beta = \left[ \frac{R_3^2 - R_2^2}{R_3^2 Z_1^2(\omega R_3) - R_2^2 Z_1^2(\omega R_2)} \right]^{1/2}, \quad (41)$$

where  $R_3$  is a solution to the equation  $Z_0(\omega R_3) \equiv 0$ , in Eq. (41) we also exploit additional cylindrical function in the following form  $Z_1(x) \equiv J_1(x) - Y_1(x)J_0(\omega R_2)/Y_0(\omega R_2)$ .

Remarkably, for above mentioned encapsulated cavity design the overlapping factor reads

$$\tilde{\mathcal{G}} = \tilde{\mathcal{G}}_3 - \tilde{\mathcal{G}}_2, \quad (42)$$

where  $\tilde{\mathcal{G}}_i$  are defined for  $i = 2, 3$  as follows

$$\tilde{\mathcal{G}}_i = \frac{L^2 \beta^2 R_1 R_i Z_1(\omega R_i)}{\omega V_{\text{rec}} V_{\text{em}}} \times \mathcal{I}_i, \quad (43)$$

here the typical integral  $\mathcal{I}_i$  can be expressed in the following form

$$\begin{aligned} \mathcal{I}_i &= \int_0^\infty dk_\rho k_\rho \frac{J_0(k_\rho R_1) J_0(k_\rho R_i)}{(k_\rho^2 - \omega^2)^2} \\ &\times \int_{-\infty}^\infty dk_z \frac{4 \sin^2(k_z L/2) (k_z^2 + m_{A'}^2)}{L^2 k_z^2 (k_\rho^2 - [k_{A'}^2 - k_z^2 + i\varepsilon])}. \quad (44) \end{aligned}$$

Next, by employing Eqs. (A3) and (A4) in Eq. (44) for the case of  $k_{A'}^2 \equiv \omega^2 - m_{A'}^2 \gtrsim 0$ , the integration over

$k_\rho$  can be split into a sum of two terms,  $\mathcal{I}_i = \mathcal{I}_i[k_z \gtrsim k_{A'}] + \mathcal{I}_i[k_z \lesssim k_{A'}]$ , where

$$\begin{aligned} \mathcal{I}_i[k_z \lesssim k_{A'}] &= i\pi k_{A'} \int_0^1 dx \left[ \frac{\sin(k_{A'} x L/2)}{(k_{A'} x L/2)} \right]^2 \quad (45) \\ &\times \frac{J_0(k_{A'} R_1 \sqrt{1-x^2}) H_0^{(1)}(k_{A'} R_i \sqrt{1-x^2})}{k_{A'}^2 x^2 + m_{A'}^2} \end{aligned}$$

is a term for the typical integration region  $k_z \lesssim k_{A'}$  in Eq. (44), and

$$\begin{aligned} \mathcal{I}_i[k_z \gtrsim k_{A'}] &= 2k_{A'} \int_1^\infty dx \left[ \frac{\sin(k_{A'} x L/2)}{(k_{A'} x L/2)} \right]^2 \quad (46) \\ &\times \frac{I_0(k_{A'} R_1 \sqrt{x^2-1}) K_0(k_{A'} R_i \sqrt{x^2-1})}{k_{A'}^2 x^2 + m_{A'}^2} \end{aligned}$$

is a term that is associated with the integration range  $k_z \gtrsim k_{A'}$  in Eq. (44). We note that both Eqs. (45) and (46) imply the variable redefinition  $k_z = x k_{A'}$ .

Finally, for  $\varkappa_{A'}^2 \equiv m_{A'}^2 - \omega^2 \gtrsim 0$  one has

$$\begin{aligned} \mathcal{I}_i &= 2\varkappa_{A'} \int_0^\infty dx \left[ \frac{\sin(\varkappa_{A'} x L/2)}{(\varkappa_{A'} x L/2)} \right]^2 \\ &\times \frac{I_0(\varkappa_{A'} R_1 \sqrt{x^2+1}) K_0(\varkappa_{A'} R_i \sqrt{x^2+1})}{\varkappa_{A'}^2 x^2 + m_{A'}^2}, \quad (47) \end{aligned}$$

where we redefine the typical variable  $k_z = \varkappa_{A'} x$ . In addition, an analytical form of Eq. (42) can be calculated for  $m_{A'} \gg \omega$  and  $R_1 \gg d$ . In particular, the asymptotic estimation of  $\tilde{\mathcal{G}}$  in the approach  $\varkappa_{A'} L \gg 1$  implies that  $(\pi a x^2)^{-1} \sin^2 a x \simeq \delta(x)$  as long as  $a \gg 1$ , therefore this results in

$$\tilde{\mathcal{G}} \propto \frac{e^{-m_{A'} d}}{m_{A'}^3}. \quad (48)$$

Next, by using an estimate (48) and (23), we obtain the typical dependence of the expected sensitivity in the following form

$$\epsilon \propto (m_{A'})^{1/2} \times e^{\frac{m_{A'} d}{2}} \quad (49)$$

for the encapsulated setup. Remarkably, Eq. (49) implies that for encapsulated setup the dependence of  $\epsilon$  on mass  $m_{A'}$  is proportional to  $\propto (m_{A'})^{1/2}$  as opposed to  $\propto (m_{A'})^{3/4}$  for the separated receiver setup, see Eq. (38).

In order to validate our results, we calculated numerically the six-dimensional integral for the overlapping factor defined by Eq. (24) in the typical regions and the parameter spaces for both distant and encapsulated receiver. The latter numerical estimates coincide fairly well with the semi-analytical results (43) and (42).

## VI. RESULTS AND DISCUSSION

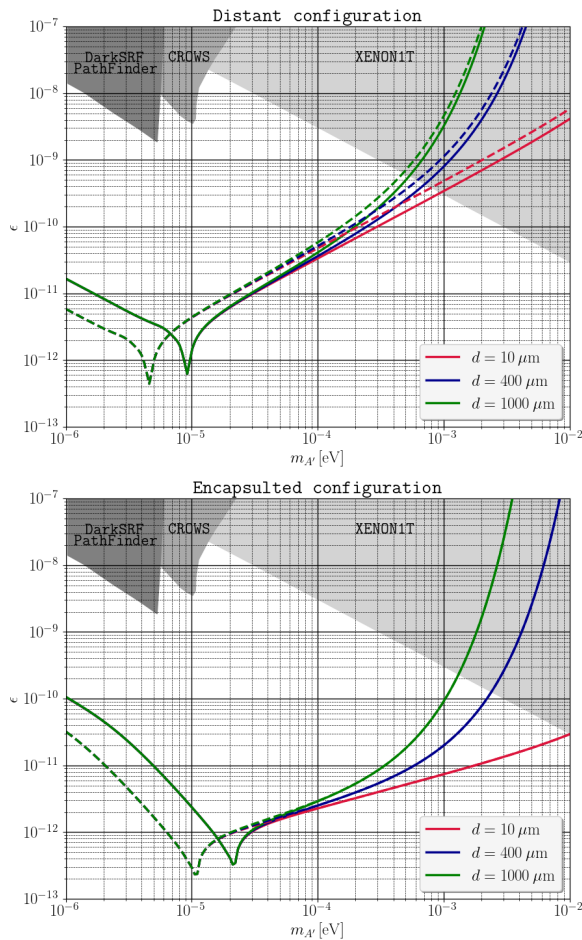


FIG. 3. The setup sensitivity to dark photon parameters for  $TM_{010}$  mode. Top panel: distant configuration, bottom panel: encapsulated configuration. The solid and dashed lines represent the typical parameters  $R = R_3 = 5$  cm,  $L = 20$  cm and  $R = R_3 = 10$  cm,  $L = 40$  cm, respectively. Green lines correspond to the typical barrier thickness of  $d = 1000$   $\mu\text{m}$ , blue lines are associated with  $d = 400$   $\mu\text{m}$ , and red lines show the ultimate limits for  $d = 10$   $\mu\text{m}$ . We set the typical setup parameters to be  $Q = 4 \times 10^{10}$ ,  $E_{\text{em}}^0 = 30$  MV/m,  $T = 4$  K, and  $t \simeq 1$  year. We also show current experimental regions that have been already ruled out by DarkSRF Pathfinder [36], CROWS [37], and XENON1T [50], these bounds were adapted from Ref. [46]

In Fig. 3 we show the sensitivities to the dark photon coupling  $\epsilon$  and mass  $m_{A'}$ , for two different choices of the experimental configurations: distant receiver (top panel) and encapsulated receiver (bottom panel). The expected reaches are shown for the barrier thickness in the range  $10$   $\mu\text{m} \lesssim d \lesssim 1$  mm. The code for numerical calculations and drawing figures can be shared upon request.

Given the benchmark geometric configuration ( $R \lesssim$

$10$  cm,  $L \lesssim 40$  cm) for distant setup the resonant enhancement of the DP sensitivity  $\epsilon \lesssim 4 \times 10^{-13}$  can be achieved for the typical masses  $5 \times 10^{-6}$  eV  $\lesssim m_{A'} \lesssim 10^{-5}$  eV. The expected reach for off-shell regime,  $m_{A'} \gg \omega$ , in this case can be as small as  $\epsilon \lesssim 5 \times 10^{-10}$  for the masses below  $m_{A'} \lesssim 10^{-3}$  eV.

The nested design of the emitter for the radius  $R_3 \lesssim 10$  cm and the typical length  $L \lesssim 40$  cm can provide the peak sensitivity at the level of  $\epsilon \lesssim 2 \times 10^{-13}$  for resonant mass region  $10^{-5}$  eV  $\lesssim m_{A'} \lesssim 2 \times 10^{-5}$  eV. The ultimate thickness of the barrier between emitter and receiver,  $d \simeq 10$   $\mu\text{m}$ , can ensure the off-shell DP,  $m_{A'} \gg \omega$ , sensitivity at the level of  $\epsilon \lesssim 10^{-11}$  for the mass range below  $m_{A'} \lesssim 10^{-2}$  eV.

It is shown in Fig. 3 that the LStinW sensitivity bound in case of off-shell dark photons,  $m_{A'} \gtrsim \omega$  can be associated with two typical regimes. The first one is associated with the mass range  $m_{A'} \gtrsim d^{-1}$  that relates to the exponential decreasing of the sensitivity. The second one is the intermediate regime for  $\omega \lesssim m_{A'} \lesssim d^{-1}$ . In this mass range the sensitivity is still high, and the typical  $\epsilon$  increases as a power low function on the dark photon mass. The slope of the curves in the encapsulated configuration is flatter than in the distant one. Thus, we can conclude that the encapsulated receiver setup can provide an enhanced sensitivity for the case of large dark photon mass and the narrow wall between cavities.

The possible extension of the present work can be addressed to a probing of axion-like particles [35, 51, 52] in LStinW setup for both distant and encapsulated receiver. We leave that task for future work.

## VII. ACKNOWLEDGEMENTS

The work on analytic and semi-analytic calculation of the setup sensitivity is supported by RSF grant no. 21-72-10151.

### Appendix A: Auxiliary integrals

In this section we summarize some helpful integrals for calculation of the form-factor  $\tilde{\mathcal{G}}$ . The first one is an indefinite integral for the product of the Bessel functions [53]

$$\int x dx z_p(\alpha x) \zeta_p(\beta x) \quad (A1)$$

$$= \frac{z_p(\alpha x) \beta x \zeta_{p-1}(\beta x) - \zeta_p(\beta x) \alpha x z_{p-1}(\alpha x)}{\alpha^2 - \beta^2},$$

where  $\alpha$  and  $\beta$  are arbitrary real numbers,  $z_p(x)$  and  $\zeta_p(x)$  are arbitrary Bessel functions of  $p^{\text{th}}$  order. The second one is the integral over the angular coordinate

$$\int_0^{2\pi} d\phi \exp[-i(k_x \rho \cos \phi + k_y \rho \sin \phi)] = 2\pi J_0(k_\rho \rho), \quad (\text{A2})$$

where  $k_\rho = (k_x^2 + k_y^2)^{1/2}$ .

One can show that for sufficiently thin wall between emitter and receiver of the encapsulated design,  $d \ll R_1$ , the following estimate for the integral holds

$$\begin{aligned} & \int_0^\infty \frac{k_\rho dk_\rho}{(k_\rho^2 - (q^2 + i\varepsilon))} \cdot \frac{J_0(k_\rho R_1) J_0(k_\rho R_i)}{(k_\rho^2 - \omega^2)^2} \\ &= \frac{i\pi}{2} \frac{J_0(qR_1) H_0^{(1)}(qR_i)}{(q^2 - \omega^2)^2}, \end{aligned} \quad (\text{A3})$$

where  $H_0^{(1)}(qR_i)(x)$  is a Hankel function of first kind,  $q^2 = k_{A'}^2 - k_z^2$ , the indices are  $i = 2, 3$ , the regarding radii  $R_i$  are be estimated to be  $R_2 \simeq R_1$  and  $R_3 \simeq R_1 x_{02}/x_{01}$ , with  $x_{01} \simeq 2.405$  and  $x_{02} \simeq 5.520$  being a first and second zero of Bessel  $J_0(x)$ , such that  $J_0(x_{01}) = J_0(x_{02}) = 0$ . For pure imaginary  $q \equiv iQ = i(\varkappa_{A'}^2 + k_z^2)^{1/2}$  the integration yields

$$\begin{aligned} & \int_0^\infty \frac{k_\rho dk_\rho}{k_\rho^2 + Q^2 - i\varepsilon} \cdot \frac{J_0(R_1 k_\rho) J_0(R_i k_\rho)}{(k_\rho^2 - \omega^2)^2} \\ &= \frac{I_0(R_1 Q) K_0(R_i Q)}{(Q^2 + \omega^2)^2}, \end{aligned} \quad (\text{A4})$$

where we imply that  $H_0^{(1)}(ix) = \frac{2}{i\pi} K_0(x)$  and  $J_0(ix) =$

$I_0(x)$  with  $K_0(x)$  and  $I_0(x)$  being a Macdonald and Infeld cylindrical (modified Bessel) functions respectively [53].

## Appendix B: Asymptotic for distant cavity design

Implying the limits  $m_{A'} \gg \omega$ ,  $m_{A'} R \gg 1$ , and  $d \ll L$  for Eq. (A4) one can show that Eq. (33) reads

$$\mathcal{I} \simeq \int_{-\infty}^{+\infty} \frac{dk_z}{2R} \frac{1}{(k_z^2 + m_{A'}^2)^{3/2}} \left[ \frac{\sin \frac{k_z L}{2}}{\frac{k_z L}{2}} \right]^2 e^{ik_z(d+L)}, \quad (\text{B1})$$

where we imply that  $\varkappa_{A'} \simeq m_{A'}$ , the above mentioned integral can be rewritten in the following form

$$\begin{aligned} \mathcal{I} &\simeq \frac{2}{RL^2 m_{A'}^4} \\ &\times [I(m_{A'}(d+2L)) + I(m_{A'}d) - 2I(m_{A'}(d+L))], \end{aligned} \quad (\text{B2})$$

where  $I(a)$  is a typical combination of the Macdonald,  $K_n(a)$ , and Struve,  $L_n(a)$ , functions [53]

$$\begin{aligned} I(a) &= -1 + \frac{a^2}{2} [K_2(a) - K_0(a) \\ &\quad + \frac{\pi}{2} K_0(a) L_{-1}(a) + \frac{\pi}{2} K_1(a) L_0(a)]. \end{aligned} \quad (\text{B3})$$

By expanding Eq. (B2) for large argument  $m_{A'} d \gg 1$  and employing Eq. (B3) one can obtain [53]

$$\mathcal{I} \simeq \frac{e^{-m_{A'} d}}{RL^2 m_{A'}^4} \left( \frac{\pi m_{A'} d}{2} \right)^{1/2} \left( 1 + \mathcal{O} \left( \frac{1}{m_{A'} d} \right) \right), \quad (\text{B4})$$

that leads to Eq. (37) for the asymptotic of the overlapping factor in case of separated cavities.

- 
- [1] Bob Holdom, “Two U(1)’s and Epsilon Charge Shifts,” *Phys. Lett. B* **166**, 196–198 (1986).
- [2] Ann E. Nelson and Jakub Scholtz, “Dark Light, Dark Matter and the Misalignment Mechanism,” *Phys. Rev. D* **84**, 103501 (2011), arXiv:1105.2812 [hep-ph].
- [3] Paola Arias, Davide Cadamuro, Mark Goodsell, Joerg Jaeckel, Javier Redondo, and Andreas Ringwald, “WISPy Cold Dark Matter,” *JCAP* **06**, 013 (2012), arXiv:1201.5902 [hep-ph].
- [4] C. Antel *et al.*, “Feebly Interacting Particles: FIPs 2022 workshop report,” *Eur. Phys. J. C* **83**, 1122 (2023), arXiv:2305.01715 [hep-ph].
- [5] Alexey S. Zhevlakov, Dmitry V. Kirpichnikov, Sergei N. Gninenko, Sergey Kuleshov, and Valery E. Lyubovitskij, “Probing invisible vector meson decay mode with the hadronic beam in the NA64 experiment at SPS CERN,” *Phys. Rev. D* **108**, 115005 (2023), arXiv:2309.09347 [hep-ph].
- [6] Yu. M. Andreev *et al.* (NA64), “Search for Light Dark Matter with NA64 at CERN,” *Phys. Rev. Lett.* **131**, 161801 (2023), arXiv:2307.02404 [hep-ex].
- [7] L. B. Okun, “LIMITS OF ELECTRODYNAMICS: PARAPHOTONS?” *Sov. Phys. JETP* **56**, 502 (1982).
- [8] J. P. Lees *et al.* (BaBar), “Search for Invisible Decays of a Dark Photon Produced in  $e^+e^-$  Collisions at BaBar,” *Phys. Rev. Lett.* **119**, 131804 (2017), arXiv:1702.03327 [hep-ex].
- [9] Roel Aaij *et al.* (LHCb), “Search for Dark Photons Produced in 13 TeV  $pp$  Collisions,” *Phys. Rev. Lett.* **120**, 061801 (2018), arXiv:1710.02867 [hep-ex].
- [10] D. Banerjee *et al.* (NA64), “Improved limits on a hypothetical X(16.7) boson and a dark photon decaying into  $e^+e^-$  pairs,” *Phys. Rev. D* **101**, 071101 (2020), arXiv:1912.11389 [hep-ex].
- [11] D. Banerjee *et al.* (NA64), “Search for a Hypothetical 16.7 MeV Gauge Boson and Dark Photons in the NA64



- Experiment at CERN,” *Phys. Rev. Lett.* **120**, 231802 (2018), [arXiv:1803.07748 \[hep-ex\]](#).
- [12] Francesco D’Eramo, Giuseppe Lucente, Newton Nath, and Seokhoon Yun, “Terrestrial detection of hidden vectors produced by solar nuclear reactions,” *JHEP* **12**, 091 (2023), [arXiv:2305.14420 \[hep-ph\]](#).
- [13] Henso Abreu *et al.* (FASER), “Search for dark photons with the FASER detector at the LHC,” *Phys. Lett. B* **848**, 138378 (2024), [arXiv:2308.05587 \[hep-ex\]](#).
- [14] E. R. Williams, J. E. Faller, and H. A. Hill, “New experimental test of Coulomb’s law: A Laboratory upper limit on the photon rest mass,” *Phys. Rev. Lett.* **26**, 721–724 (1971).
- [15] S. A. Abel, M. D. Goodsell, J. Jaeckel, V. V. Khoze, and A. Ringwald, “Kinetic Mixing of the Photon with Hidden U(1)s in String Phenomenology,” *JHEP* **07**, 124 (2008), [arXiv:0803.1449 \[hep-ph\]](#).
- [16] Joerg Jaeckel and Sabyasachi Roy, “Spectroscopy as a test of Coulomb’s law: A Probe of the hidden sector,” *Phys. Rev. D* **82**, 125020 (2010), [arXiv:1008.3536 \[hep-ph\]](#).
- [17] Graciela B. Gelmini, Alexander J. Millar, Volodymyr Takhistov, and Edoardo Vitagliano, “Probing dark photons with plasma haloscopes,” *Phys. Rev. D* **102**, 043003 (2020), [arXiv:2006.06836 \[hep-ph\]](#).
- [18] Jesse Liu *et al.* (BREAD), “Broadband Solenoidal Haloscope for Terahertz Axion Detection,” *Phys. Rev. Lett.* **128**, 131801 (2022), [arXiv:2111.12103 \[physics.ins-det\]](#).
- [19] Jeff Chiles *et al.*, “New Constraints on Dark Photon Dark Matter with Superconducting Nanowire Detectors in an Optical Haloscope,” *Phys. Rev. Lett.* **128**, 231802 (2022), [arXiv:2110.01582 \[hep-ex\]](#).
- [20] Yifan Chen, Chunlong Li, Yuxiang Liu, Yuxin Liu, Jing Shu, and Yanjie Zeng, “SRF Cavity as Galactic Dark Photon Telescope,” (2024), [arXiv:2402.03432 \[hep-ph\]](#).
- [21] Stefan Knirck *et al.*, “First Results from a Broadband Search for Dark Photon Dark Matter in the 44 to 52  $\mu\text{eV}$  range with a coaxial dish antenna,” (2023), [arXiv:2310.13891 \[hep-ex\]](#).
- [22] Saptarshi Chaudhuri, Peter W. Graham, Kent Irwin, Jeremy Mardon, Surjeet Rajendran, and Yue Zhao, “Radio for hidden-photon dark matter detection,” *Phys. Rev. D* **92**, 075012 (2015), [arXiv:1411.7382 \[hep-ph\]](#).
- [23] David Alesini *et al.*, “The future search for low-frequency axions and new physics with the FLASH resonant cavity experiment at Frascati National Laboratories,” *Phys. Dark Univ.* **42**, 101370 (2023), [arXiv:2309.00351 \[physics.ins-det\]](#).
- [24] Ben T. McAllister, Aaron Quiskamp, Ciaran A. J. O’Hare, Paul Altin, Eugene N. Ivanov, Maxim Goryachev, and Michael E. Tobar, “Limits on Dark Photons, Scalars, and Axion-Electromagnetodynamics with the ORGAN Experiment,” *Annalen Phys.* **536**, 2200622 (2024), [arXiv:2212.01971 \[hep-ph\]](#).
- [25] Zhenxing Tang *et al.*, “SRF Cavity Searches for Dark Photon Dark Matter: First Scan Results,” (2023), [arXiv:2305.09711 \[hep-ex\]](#).
- [26] M. Afif Ismail, Chrisna Setyo Nugroho, and Henry Tsz-King Wong, “Exploring dark photons via a subfrequency laser search in gravitational wave detectors,” *Phys. Rev. D* **107**, 082002 (2023), [arXiv:2211.13384 \[hep-ph\]](#).
- [27] Shumpei Kotaka *et al.* (DOSUE-RR), “Search for Dark Photon Dark Matter in the Mass Range 74–110  $\mu\text{eV}$  with a Cryogenic Millimeter-Wave Receiver,” *Phys. Rev. Lett.* **130**, 071805 (2023), [arXiv:2205.03679 \[hep-ex\]](#).
- [28] Dieter Horns, Joerg Jaeckel, Axel Lindner, Andrei Lobanov, Javier Redondo, and Andreas Ringwald, “Searching for WISPy Cold Dark Matter with a Dish Antenna,” *JCAP* **04**, 016 (2013), [arXiv:1212.2970 \[hep-ph\]](#).
- [29] Haipeng An, Fa Peng Huang, Jia Liu, and Wei Xue, “Radio-frequency Dark Photon Dark Matter across the Sun,” *Phys. Rev. Lett.* **126**, 181102 (2021), [arXiv:2010.15836 \[hep-ph\]](#).
- [30] Michael L. Graesser, R. Andrew Gustafson, Kate Hildebrandt, Varun Mathur, and Ian M. Shoemaker, “Detecting Boosted Dark Photons with Gaseous Detectors,” (2024), [arXiv:2402.00941 \[hep-ph\]](#).
- [31] Nikita Blinov, Christina Gao, Roni Harnik, Ryan Janish, and Neil Sinclair, “Dark Matter Searches on a Photonic Chip,” (2024), [arXiv:2401.17260 \[hep-ph\]](#).
- [32] Nirmalya Brahma, Asher Berlin, and Katelin Schutz, “Photon-dark photon conversion with multiple level crossings,” *Phys. Rev. D* **108**, 095045 (2023), [arXiv:2308.08586 \[hep-ph\]](#).
- [33] Itay M. Bloch and Saarik Kalia, “Curl up with a good B: detecting ultralight dark matter with differential magnetometry,” *JHEP* **24**, 178 (2020), [arXiv:2308.10931 \[hep-ph\]](#).
- [34] Michael A. Fedderke, Peter W. Graham, Derek F. Jackson Kimball, and Saarik Kalia, “Earth as a transducer for dark-photon dark-matter detection,” *Phys. Rev. D* **104**, 075023 (2021), [arXiv:2106.00022 \[hep-ph\]](#).
- [35] Asher Berlin *et al.*, “Searches for New Particles, Dark Matter, and Gravitational Waves with SRF Cavities,” (2022), [arXiv:2203.12714 \[hep-ph\]](#).
- [36] A. Romanenko *et al.*, “Search for Dark Photons with Superconducting Radio Frequency Cavities,” *Phys. Rev. Lett.* **130**, 261801 (2023), [arXiv:2301.11512 \[hep-ex\]](#).
- [37] M. Betz, F. Caspers, M. Gasior, M. Thumm, and S. W. Rieger, “First results of the CERN Resonant Weakly Interacting sub-eV Particle Search (CROWS),” *Phys. Rev. D* **88**, 075014 (2013), [arXiv:1310.8098 \[physics.ins-det\]](#).
- [38] A. Wagner *et al.* (ADMX), “A Search for Hidden Sector Photons with ADMX,” *Phys. Rev. Lett.* **105**, 171801 (2010), [arXiv:1007.3766 \[hep-ex\]](#).
- [39] Rhys Povey, John Hartnett, and Michael Tobar, “Microwave cavity light shining through a wall optimization and experiment,” *Phys. Rev. D* **82**, 052003 (2010), [arXiv:1003.0964 \[hep-ex\]](#).
- [40] K. Van Bibber, N. R. Dagdeviren, S. E. Koonin, A. Kerman, and H. N. Nelson, “Proposed experiment to produce and detect light pseudoscalars,” *Phys. Rev. Lett.* **59**, 759–762 (1987).

- [41] Joerg Jaeckel and Andreas Ringwald, “A Cavity Experiment to Search for Hidden Sector Photons,” *Phys. Lett. B* **659**, 509–514 (2008), [arXiv:0707.2063 \[hep-ph\]](#).
- [42] Peter W. Graham, Jeremy Mardon, Surjeet Rajendran, and Yue Zhao, “Parametrically enhanced hidden photon search,” *Phys. Rev. D* **90**, 075017 (2014), [arXiv:1407.4806 \[hep-ph\]](#).
- [43] Younggeun Kim, SungWoo Youn, Danho Ahn, Junu Jung, Dongok Kim, and Yannis K. Semertzidis, “Sensitivity improvement in hidden photon detection using resonant cavities,” *Phys. Rev. D* **103**, 055004 (2021), [arXiv:2011.14559 \[hep-ex\]](#).
- [44] Stephen R. Parker, John G. Hartnett, Rhys G. Povey, and Michael E. Tobar, “Cryogenic resonant microwave cavity searches for hidden sector photons,” *Phys. Rev. D* **88**, 112004 (2013), [arXiv:1410.5244 \[hep-ex\]](#).
- [45] Stephen R. Parker, Gray Rybka, and Michael E. Tobar, “Hidden Sector Photon Coupling of Resonant Cavities,” *Phys. Rev. D* **87**, 115008 (2013), [arXiv:1304.6866 \[hep-ph\]](#).
- [46] Asher Berlin, Roni Harnik, and Ryan Janish, “Light Shining Through a Thin Wall: Evanescent Hidden Photon Detection,” (2023), [arXiv:2303.00014 \[hep-ph\]](#).
- [47] David Hill, “Electromagnetic fields in cavities: Deterministic and statistical theories,” *Antennas and Propagation Magazine, IEEE* **56**, 306–306 (2014).
- [48] Asher Berlin, Diego Blas, Raffaele Tito D’Agnolo, Sebastian A. R. Ellis, Roni Harnik, Yonatan Kahn, and Jan Schütte-Engel, “Detecting high-frequency gravitational waves with microwave cavities,” *Phys. Rev. D* **105**, 116011 (2022), [arXiv:2112.11465 \[hep-ph\]](#).
- [49] R. H. Dicke, “The Measurement of Thermal Radiation at Microwave Frequencies,” *Rev. Sci. Instrum.* **17**, 268–275 (1946).
- [50] Haipeng An, Maxim Pospelov, Josef Pradler, and Adam Ritz, “New limits on dark photons from solar emission and keV scale dark matter,” *Phys. Rev. D* **102**, 115022 (2020), [arXiv:2006.13929 \[hep-ph\]](#).
- [51] Dmitry Salnikov, Petr Satunin, Maxim Fitkevich, and D. V. Kirpichnikov, “Light-Shining-Through-Wall Cavity Setups for Probing Axion-Like Particles,” *JETP Lett.* **117**, 889–897 (2023), [arXiv:2303.15996 \[hep-ph\]](#).
- [52] Christina Gao and Roni Harnik, “Axion searches with two superconducting radio-frequency cavities,” *JHEP* **07**, 053 (2021), [arXiv:2011.01350 \[hep-ph\]](#).
- [53] I. S. Gradshteyn and I. M. Ryzhik, *Table of Integrals, Series, and Products* (1943).